Supporting Information

Preparation and Modulation of Temperature-Responsive Multicolor Phosphorescent Materials

Yunan Liu[a], Wensheng Xu[a], Jiang Liu[a], Ligong Chen[a,b,e.], Yang Li[a,b,e], Xilong Yan [a,b,e], Jianchao Ma[c], Yin Xiao[d], Linshuo Jiang[d], Bowei Wang*[,a,b,e]

[a] School of Chemical Engineering and Technology, Tianjin University, Tianjin 300350, P. R. China.

[b] Zhejiang Institute of Tianjin University, Shaoxing, 312300, P. R. China.

[c] College of Mining Engineering, Taiyuan University of Technology, Taiyuan 030024, China.

[d] College of Chemistry and Chemical Engineering, Yulin University, Yulin 719000, China.

[e] Tianjin Key Laboratory of Applied Catalysis Science and Technology, Tianjin 300350, China.

* Corresponding author at: School of Chemical Engineering and Technology, Tianjin University, Tianjin 300350, P. R. China.

E-mail: bwwang@tju.edu.cn (Bowei Wang, ORCID ID: 0000-0002-9400-0698);

Material Characterization

FTIR spectra were recorded on an FEI iS-50 Fourier transform infrared spectrometer. Thermogravimetric analysis (TGA) was conducted using a NETZSCH TG 209F3 thermogravimetric analyzer under a nitrogen atmosphere, with the

temperature ramped from 35 to 800 °C at a heating rate of 10 °C·min^{-1}. UV-Vis absorption spectra were measured by a Shimadzu UV-1800 UV-Vis-NIR spectrophotometer. X-ray diffraction (XRD) patterns were obtained via a PANalytical B.V. XPERTPRO diffractometer. Room-temperature phosphorescence (RTP) spectra, phosphorescence lifetimes, fluorescence spectra and corresponding films afterglow were collected on an F-4700 FL photoluminescence spectrometer. Photoluminescence quantum yields were determined with an Edinburgh FLS1000 fluorescence spectrophotometer equipped with an integrating sphere.

Theoretical calculation details

For the theoretical simulations, the optimized ground-state (S_0) geometries of monomers and multimers were calculated with the ωB97XD functional and 6-311G(d,p) basis set, and no imaginary frequencies were found in the frequency analysis of the optimized structures. The energies of singlet (S_n) and triplet (T_n) excited states were obtained with time-dependent density functional theory (TD-DFT) at the same theoretical level. All the above calculations were performed by Gaussian 16, Revision C.01 package in the Paratera parallel supercomputing platform. Based on the optimized geometries, the spin-orbit coupling (SOC) matrix elements between S_1 and T_n states were calculated by ORCA 5.0.3. [1]

Preparation of 1,4-BDBA@HPD Samples

Take 1,4-BDBA @HPD (1:3) as an example. A mixture of 0.0828 g (0.5 mmol) of 1,4-phenylenebisboronic acid (1,4-BDBA) and 0.1590 g (1.5 mmol) of 2-(hydroxymethyl)-1,3-propanediol (HPD) was dispersed in 25 mL of dichloromethane (DCM). The mixture was refluxed and stirred for 4 h. After completion of the reaction, the solvent was removed under reduced pressure at 40 °C, and the sample was washed with methanol. The as-prepared product was dried in a vacuum oven at 60 °C for 12 h, yielding a white powder (0.120 g, 78.4% yield).

1,4-BDBA @HPD samples with molar ratios of 1:2, 1:4, 1:5, and 1:6 were similarly prepared as described above.

Preparation of 1,4-BDBA@HPD/PMMA afterglow film

A molar ratio of 1:3 was maintained for 1,4-phenylenebisboronic acid (1,4-BDBA,

0.034 g, 0.2 mmol) and 2-(hydroxymethyl)-1,3-propanediol (HPD, 0.066 g, 0.6 mmol), which were dispersed in 20 mL of dichloromethane. The mixture was then refluxed for 4 h to complete the reaction. After the reaction, the mixture was cooled to room temperature, and 5 mL of acetone was added subsequently. The resulting mixture was sonicated for 10 min to form a homogeneous and transparent solution.

This solution was equally divided into five 5 mL aliquots, and different masses of poly(methyl methacrylate) (PMMA, 0.40 g, 0.20 g, 0.13 g, 0.10 g) were added to each aliquot respectively. Each mixture was sonicated for 15 min until it became clear and transparent, then poured into silicone molds and dried in a forced-air oven at 40 °C for 30 min. Thus, 1,4-BDBA @HPD/PMMA composite films with doping contents of 5%, 10%, 15%, and 20% (w/w, based on the mass of PMMA) were obtained.

Preparation of Multicolor Afterglow Films Based on TS-FRET

Taking Rh110/1,4-BDBA @HPD/PMMA film as an example, 0.1 g of 1,4-BDBA @HPD (1:3) was dispersed in a mixed solvent of 20 mL dichloromethane and 5 mL acetone, followed by the addition of 1.0 g poly(methyl methacrylate) (PMMA, Mw = 120000 g/mol), and the mixture was sonicated for 15 min to ensure complete dissolution. Subsequently, 1 mg of rhodamine 110 (Rh110) dissolved in acetone to form a 0.2 mg/mL solution was added dropwise into the above mixture, with a mass fraction of 0.01%–0.1% relative to PMMA. The solution was sonicated for 5 min to achieve homogeneous mixing, poured into a silicone mold (20 mm × 20 mm × 2 mm), and dried in a forced-air oven at 40 °C for 30 min to form a film.

Rh123/1,4-BDBA @HPD/PMMA and Rh6G/1,4-BDBA @HPD/PMMA afterglow films were similarly prepared as above.

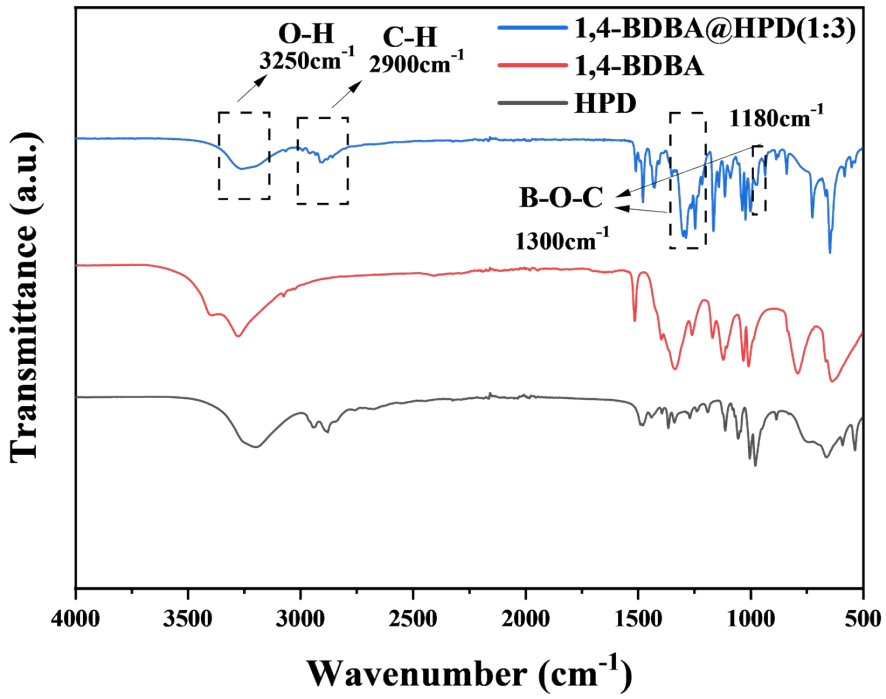

Figure S1. FTIR spectra of 1,4-BDBA @HPD sample with optimal molar ratio and raw materials.

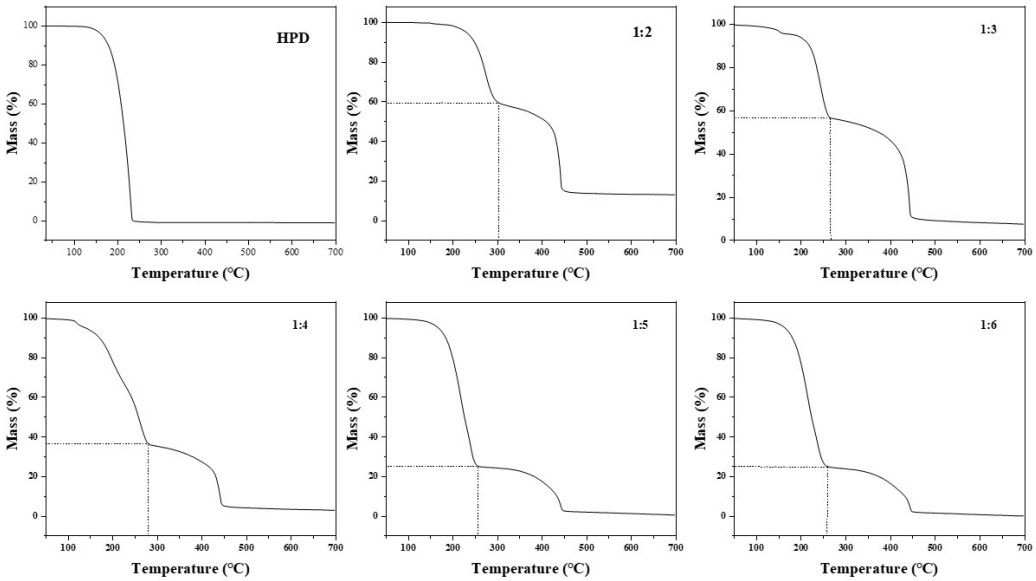

Figure S2. TGA of HPD and 1,4-BDBA @HPD with different molar ratios.

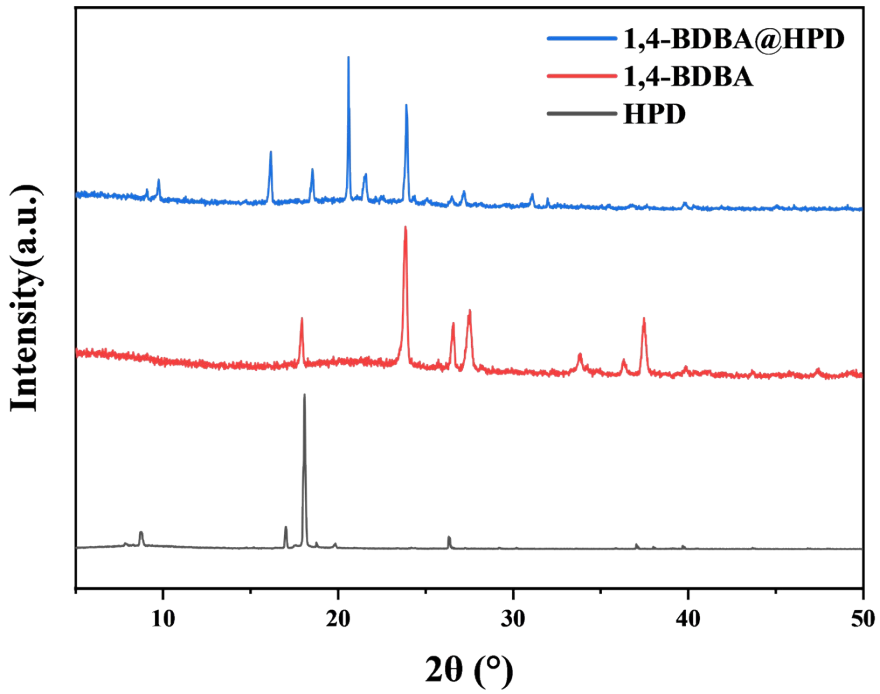

Figure S3. XRD patterns of 1,4-BDBA@HPD sample with optimal molar ratio and raw materials.

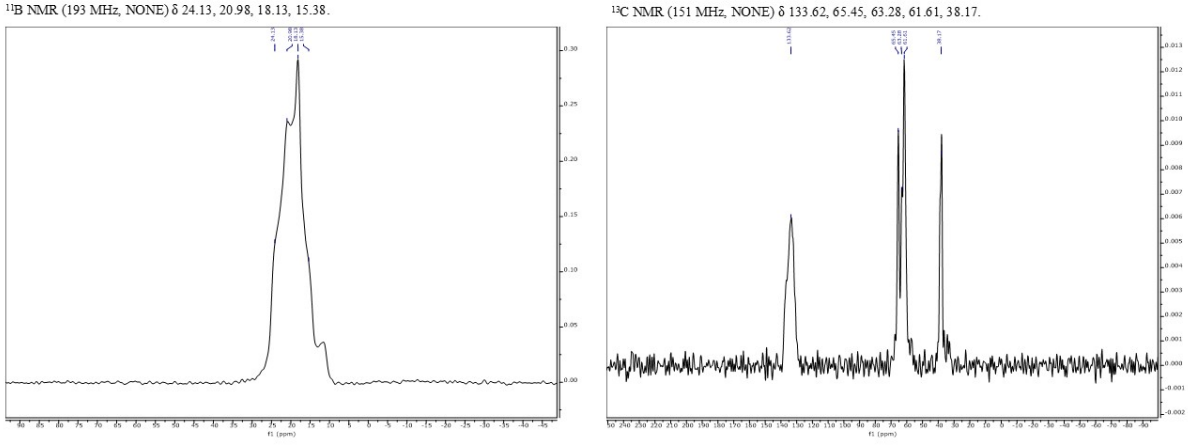

Figure S4. High-resolution ^{11}B MAS NMR and ^{13}C CP/MAS NMR spectra of 1,4-BDBA@HPD.

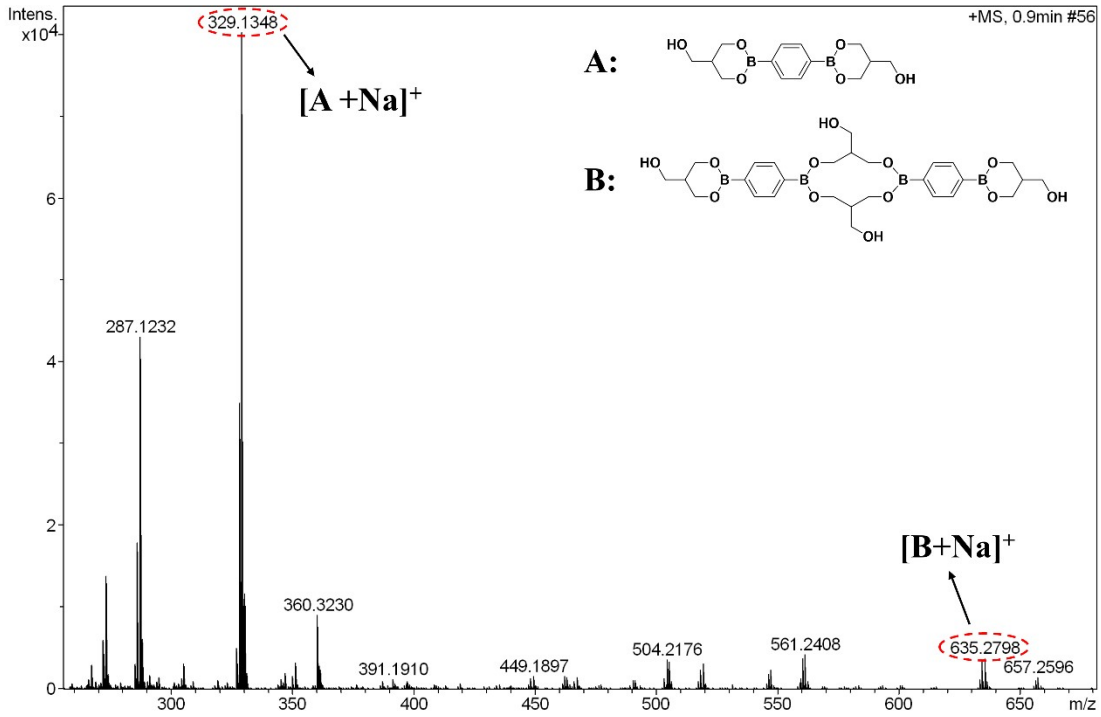

Figure S5. High-resolution mass spectrometry of 1,4-BDBA@HPD.

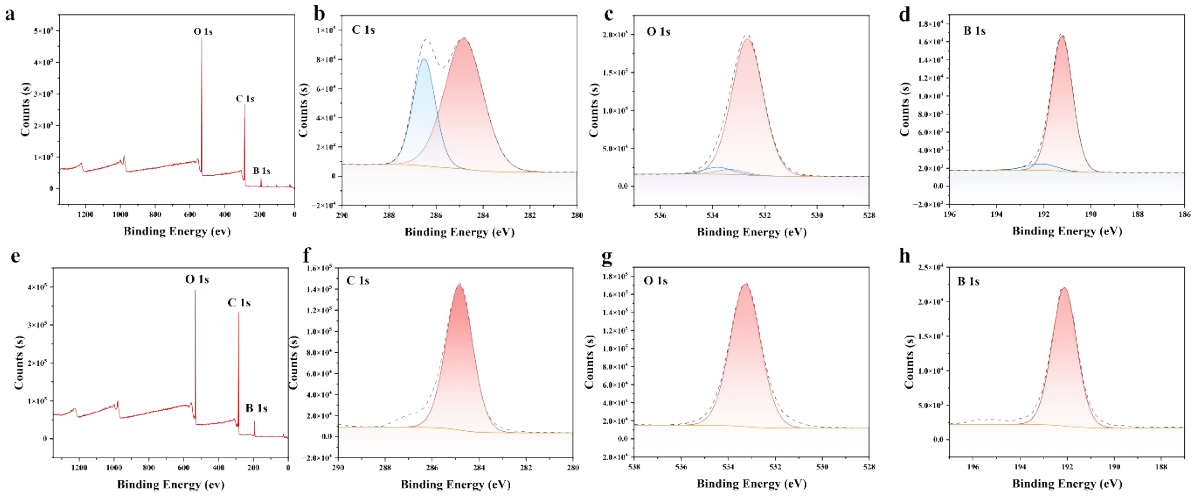

Figure S6. XPS spectra of 1,4-BDBA@HPD composite and pure 1,4-BDBA monomer. (a) Survey scan spectrum, (b) high-resolution C 1s, (c) high-resolution O 1s, (d) high-resolution B 1s of 1,4-BDBA@HPD; (e) survey scan spectrum, (f) high-resolution C 1s, (g) high-resolution O 1s, (h) high-resolution B 1s of pure 1,4-BDBA.

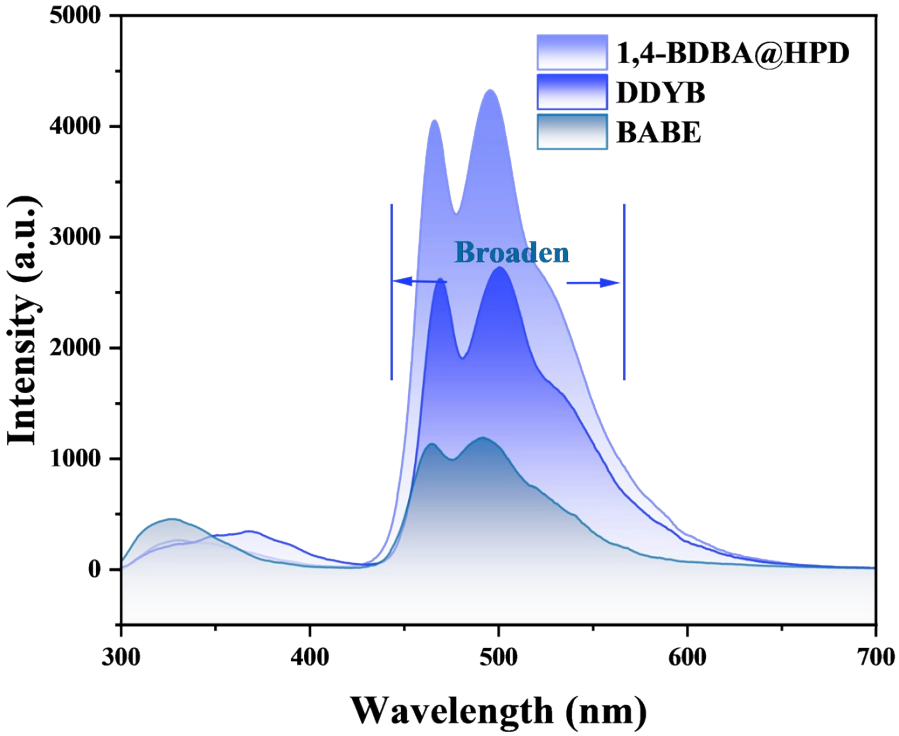

Figure S7. Comparison of delayed PL spectra among 1,4-BDBA @HPD, 1,4-Benzenediboronic Acid Bis(neopentyl glycol) Ester (BABE), and 1,4-Di(1,3,2-dioxaborinan-2-yl)benzene (DDYB).

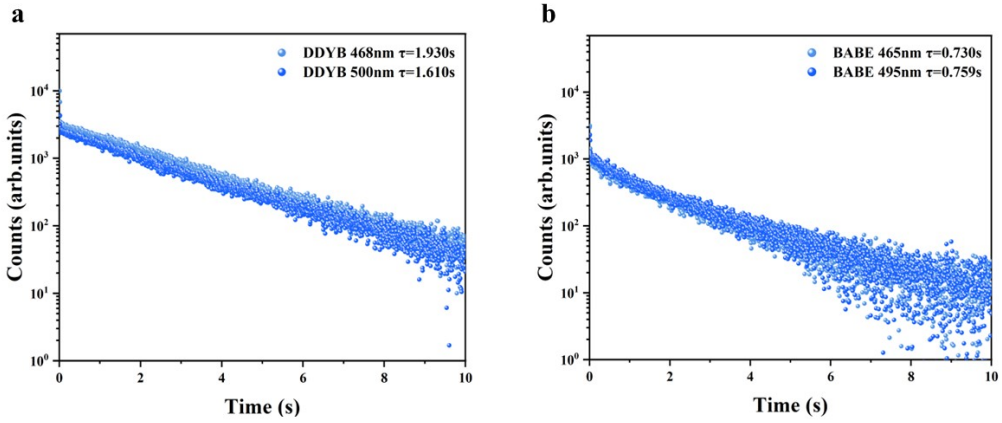

Figure S8. Lifetime decay profiles of DDYB and BABE at 468 nm, 500 nm and 465 nm, 495 nm.

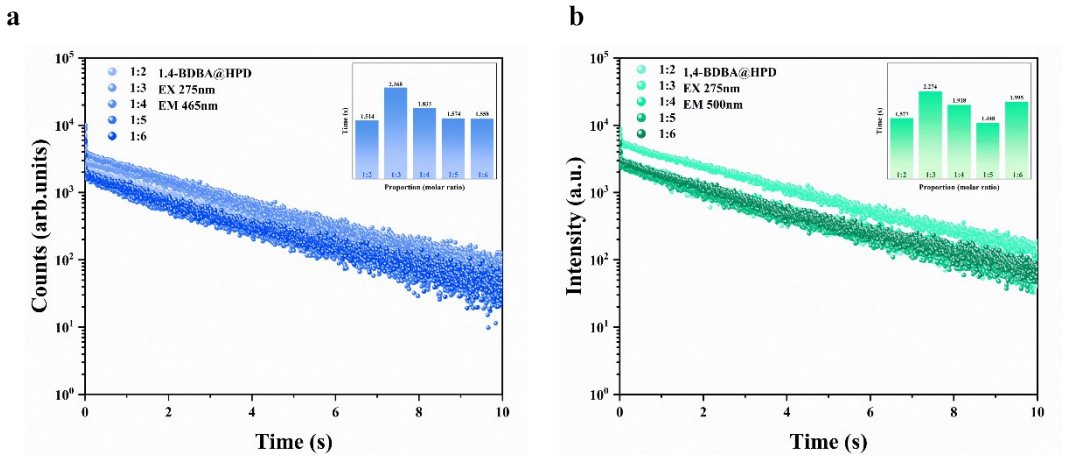

Figure S9. Lifetime decay profiles of 1,4-BDBA@HPD samples with different molar ratios at 500 nm and 465 nm under 275 nm light excitation.

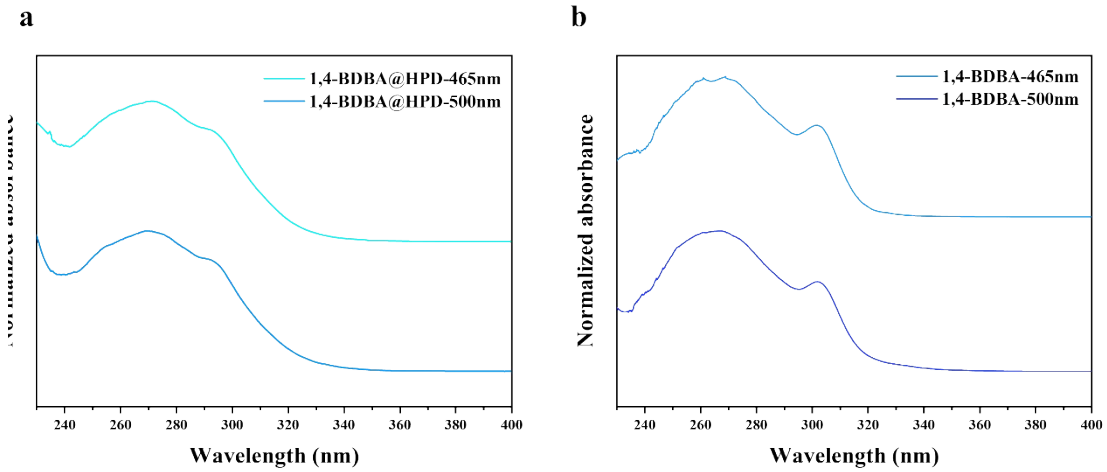

Figure S10. a) Excitation spectra of 1,4-BDBA@HPD at the optimal molar ratio at 465 nm and 500 nm; b) Excitation spectra of 1,4-BDBA at 465 nm and 500 nm.

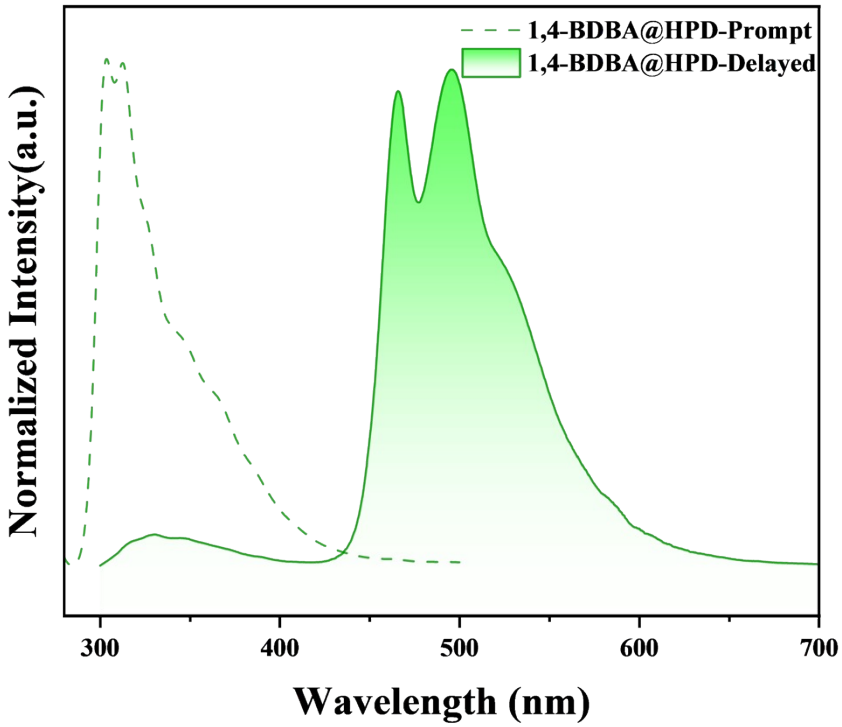

Figure S11. Delayed and prompt PL spectra of 1,4-BDBA @HPD.

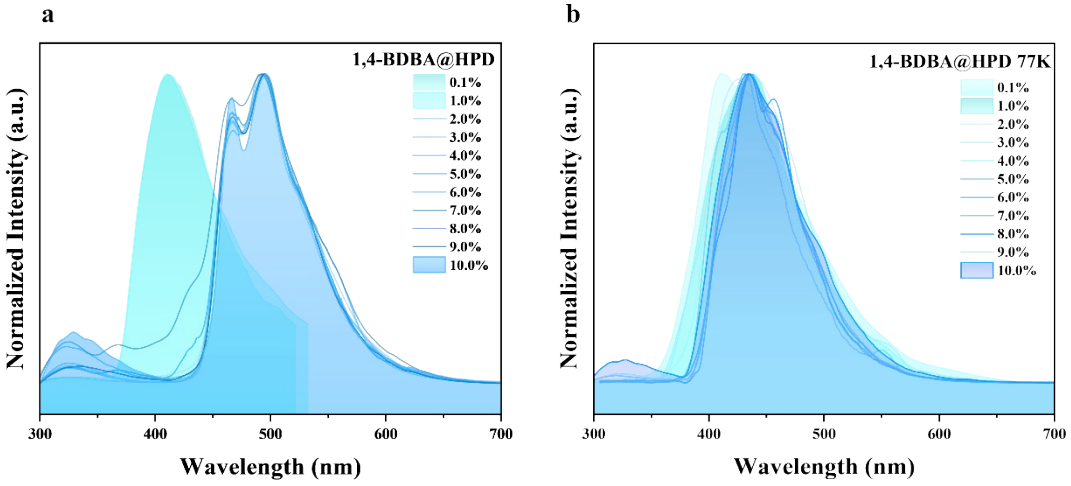

Figure S12. (a) Room-temperature delayed PL spectra of 1,4-BDBA@HPD samples with guest molecule ratios of 0.1%, from 1.0% to 10.0%. (b) Delayed PL spectra of 1,4-BDBA @HPD samples with guest molecule ratios of 0.1%, from 1.0% to 10.0% at 77 K.

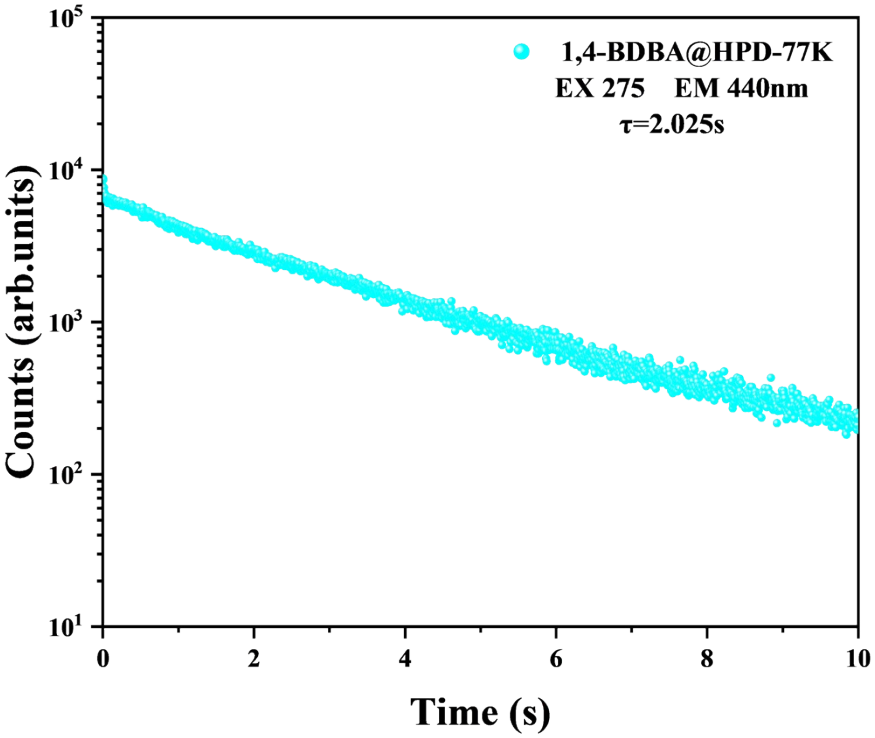

Figure S13. Lifetime decay profiles of 1,4-BDBA @HPD at the 1:3 ratio at 440 nm under 77 K.

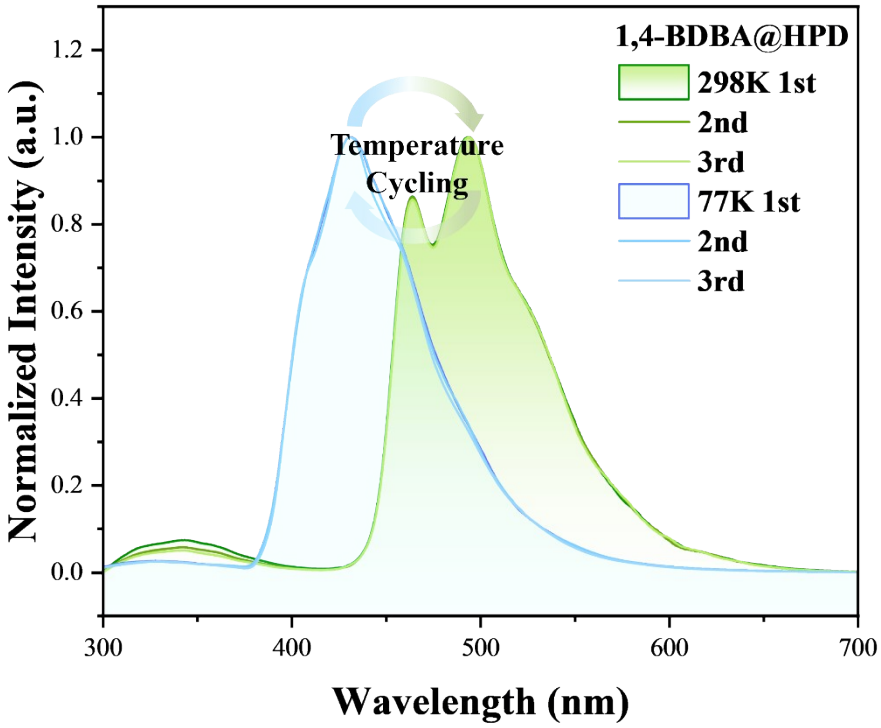

Figure S14. Delayed PL spectra of 1,4-BDBA@HPD at 77 K–298 K temperature cycles.

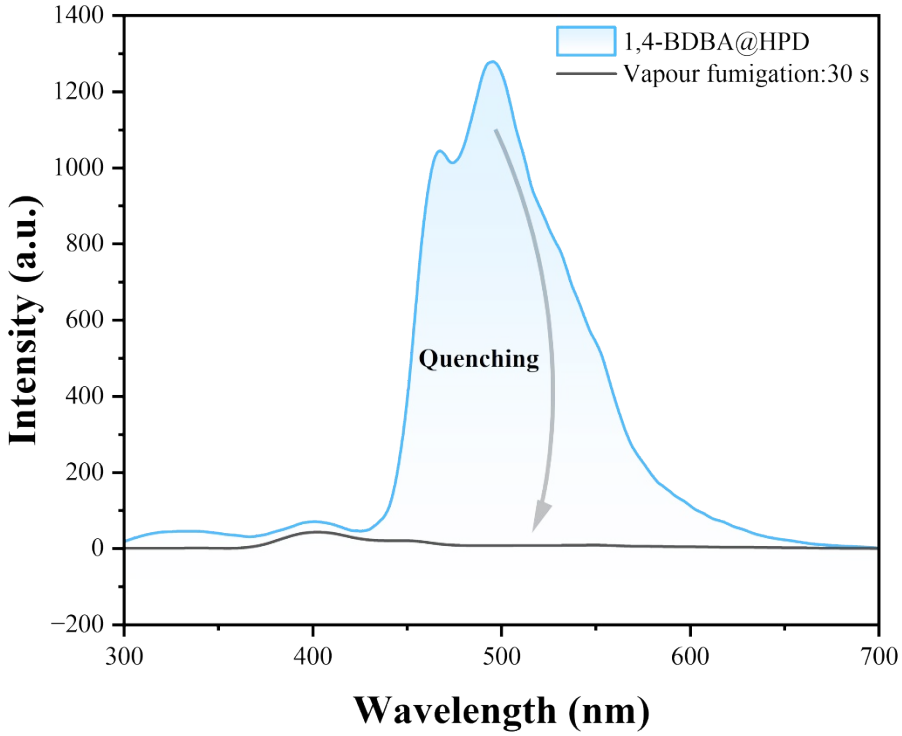

Figure S15. Delayed PL spectra of 1,4-BDBA@HPD before and after water vapour fumigation for 30 s.

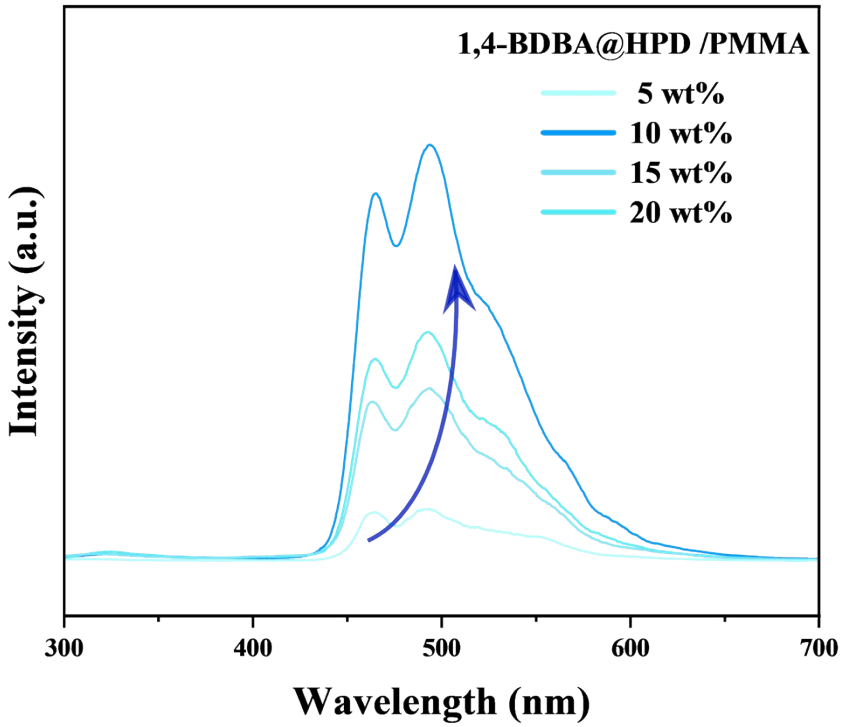

Figure S16. Delayed PL spectra of 1,4-BDBA @HPD doped in PMMA with different mass ratios.

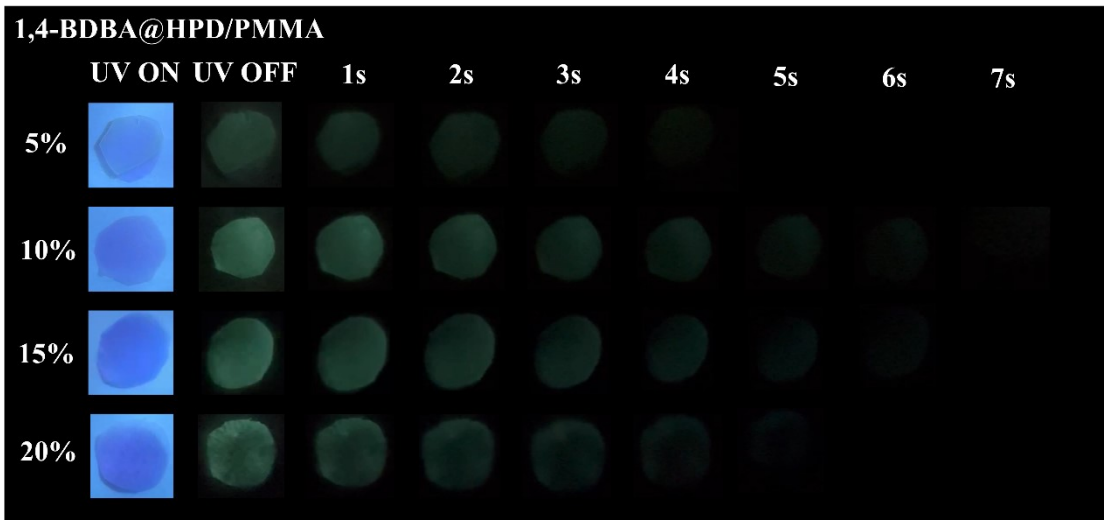

Figure S17. Photographs of 1,4-BDBA @HPD/PMMA films with different 1,4-BDBA @HPD doping contents.

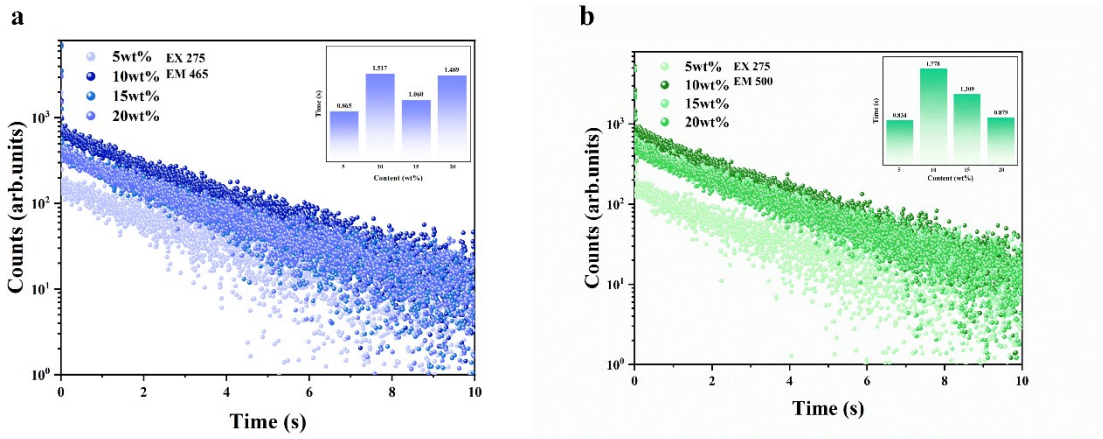

Figure S18. Lifetime decay curves at 465 nm (a) and 500 nm (b) of 1,4-BDBA @HPD doped in PMMA under 275 nm excitation.

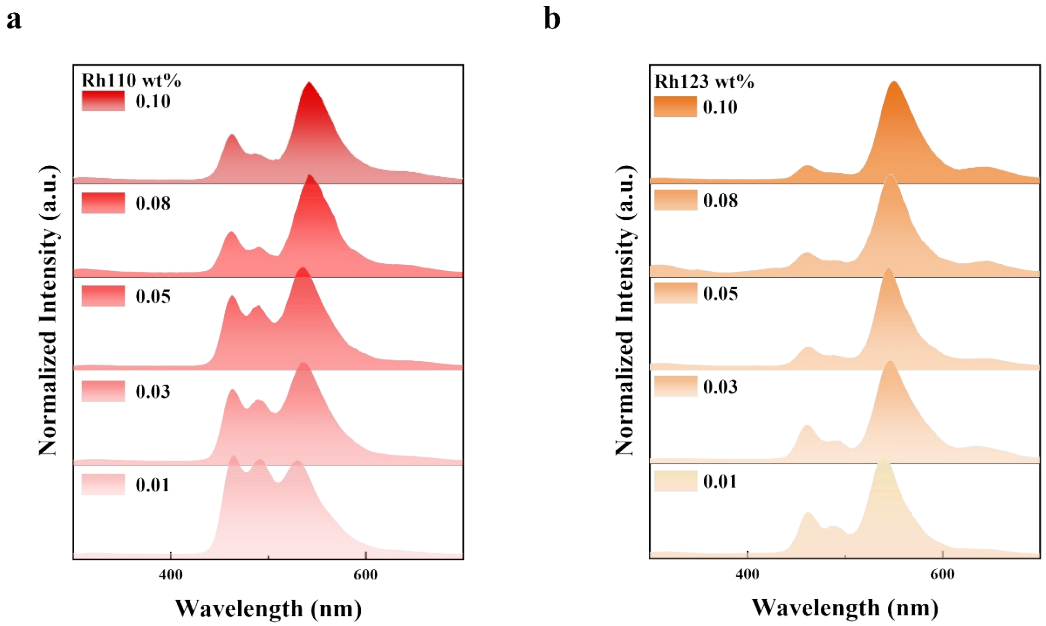

Figure S19. Normalized delayed PL spectra of afterglow films: (a) Rh110/1,4-BDBA @HPD/PMMA and (b) Rh123/1,4-BDBA @HPD/PMMA.

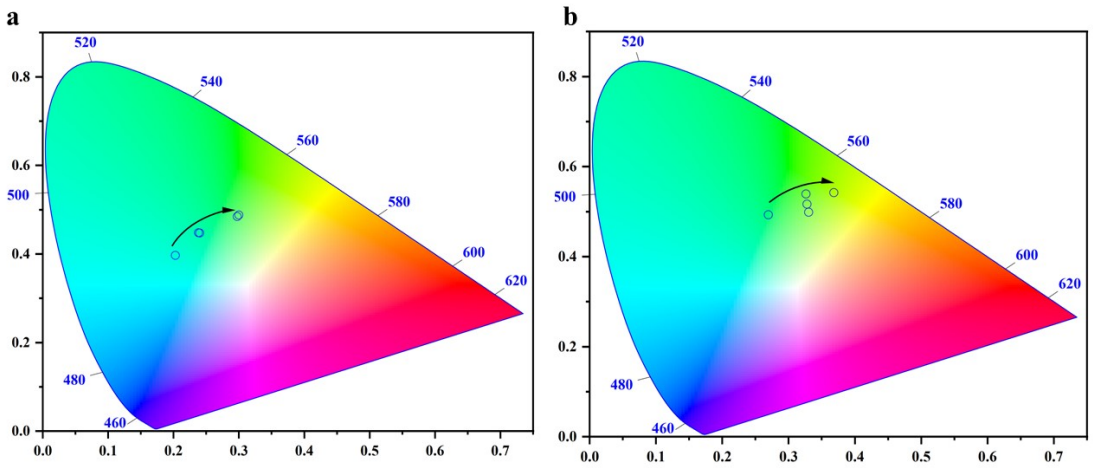

Figure S20. CIE 1931 Coordinates of afterglow films: (a) Rh110/1,4-BDBA @HPD/PMMA and (b) Rh123/1,4-BDBA @HPD/PMMA.

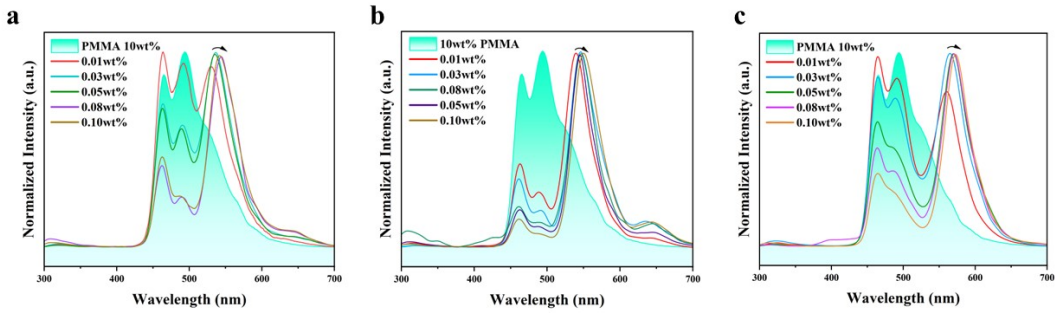

Figure S21. Delayed PL spectra of gradient-doped afterglow films: 1,4-BDBA @HPD/PMMA, (a) Rh110/1,4-BDBA @HPD/PMMA, (b) Rh123/1,4-BDBA @HPD/PMMA, and (c) Rh6G/1,4-BDBA @HPD/PMMA.

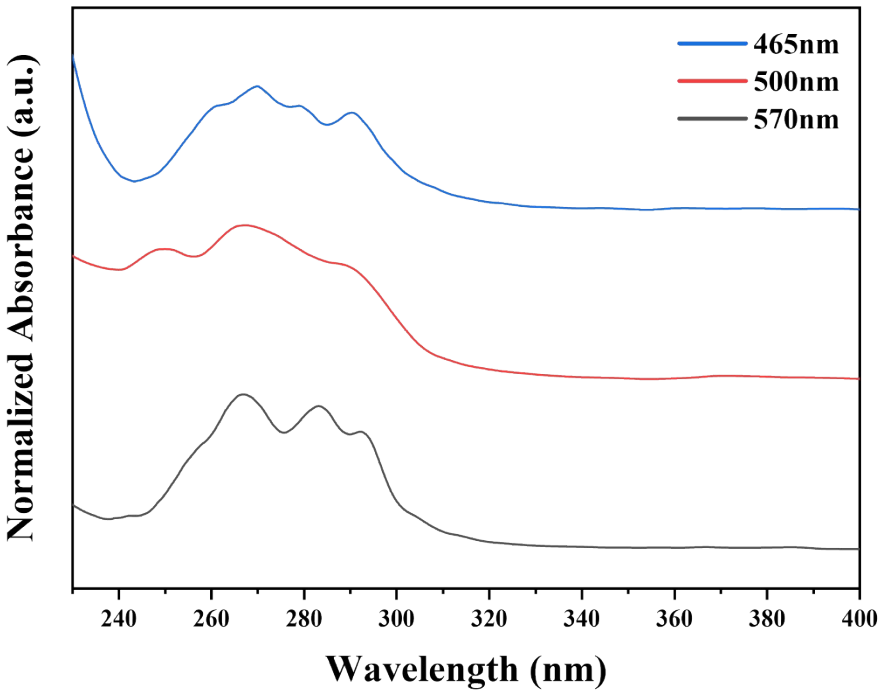

Figure S22. Delayed excitation spectra of Rh6G/1,4-BDBA @HPD/PMMA.

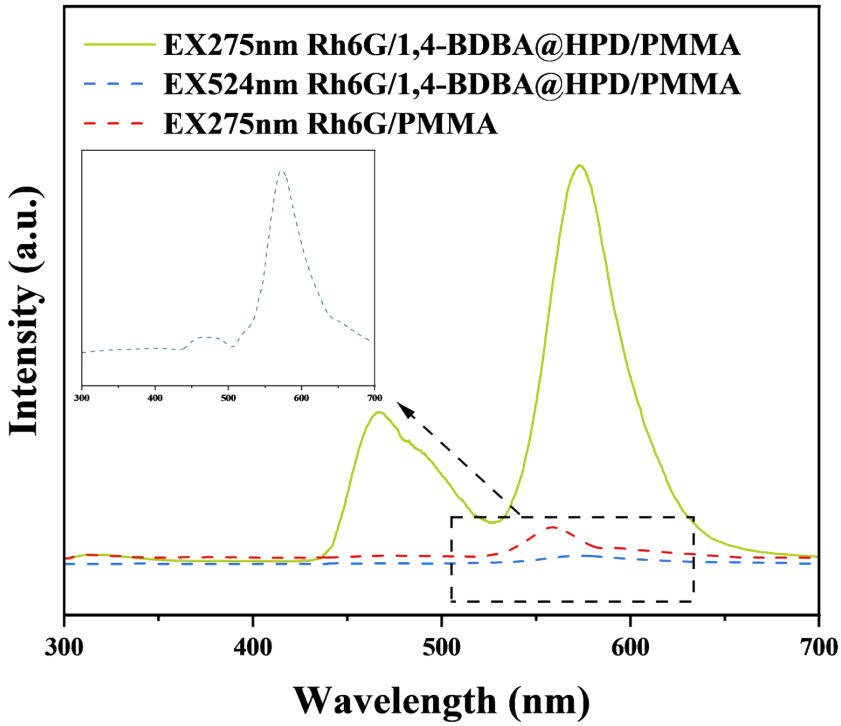

Figure S23. Delayed PL spectra of Rh6G/1,4-BDBA @HPD/PMMA at 275 nm and 524 nm, and Rh6G/PMMA at 275 nm.

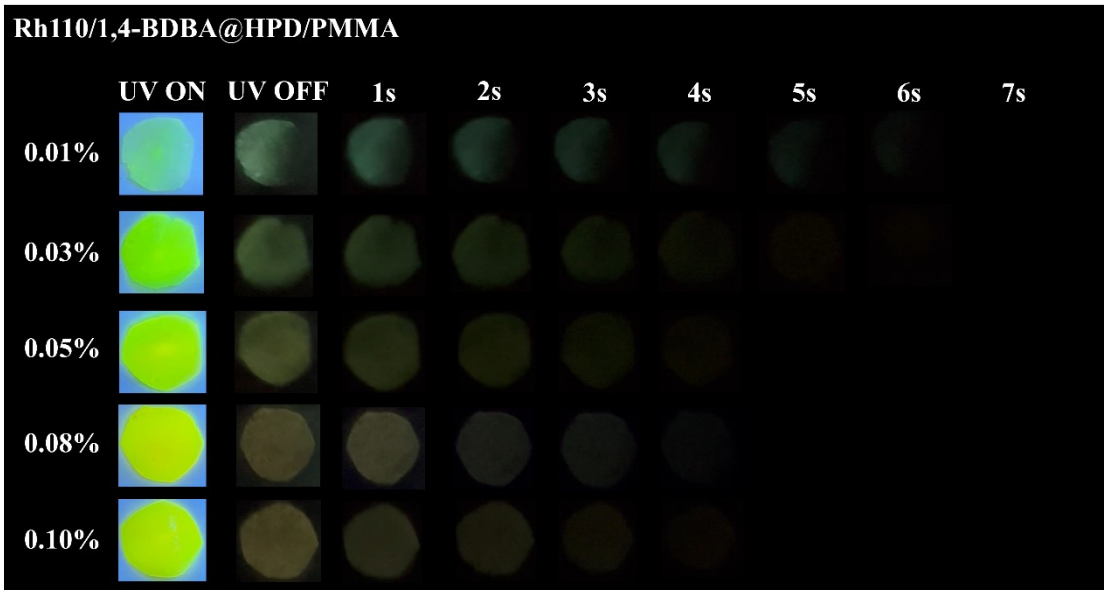

Figure S24. Afterglow photographs of Rh110/1,4-BDBA @HPD/PMMA films with different dye doping amounts under 275 nm excitation.

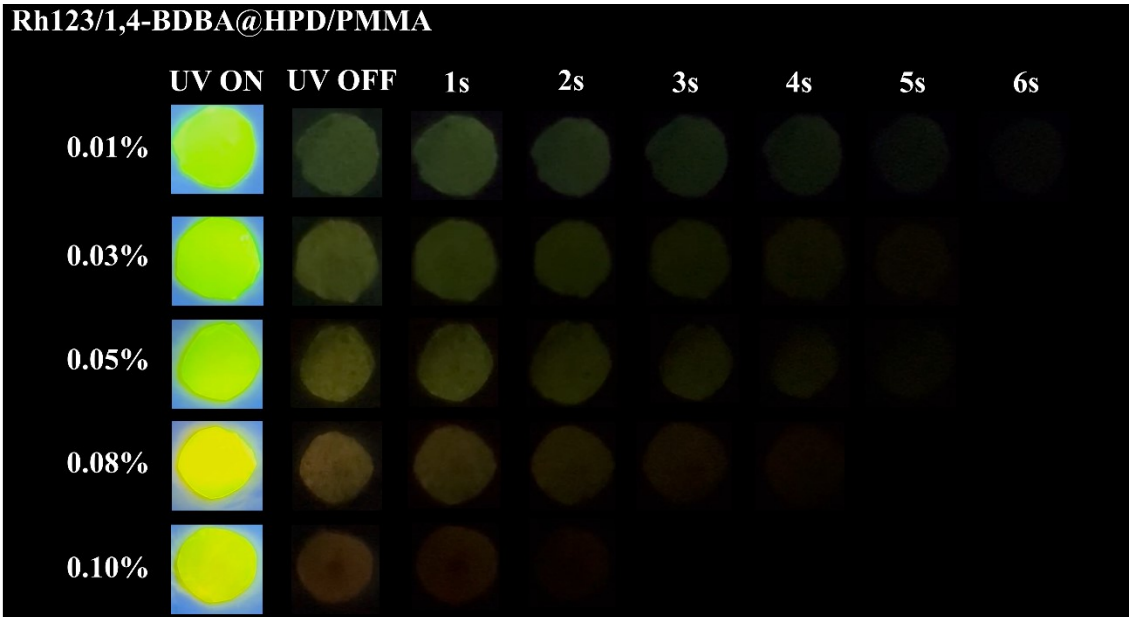

Figure S25. Afterglow photographs of Rh123/1,4-BDBA @HPD/PMMA films with different dye doping amounts under 275 nm excitation.

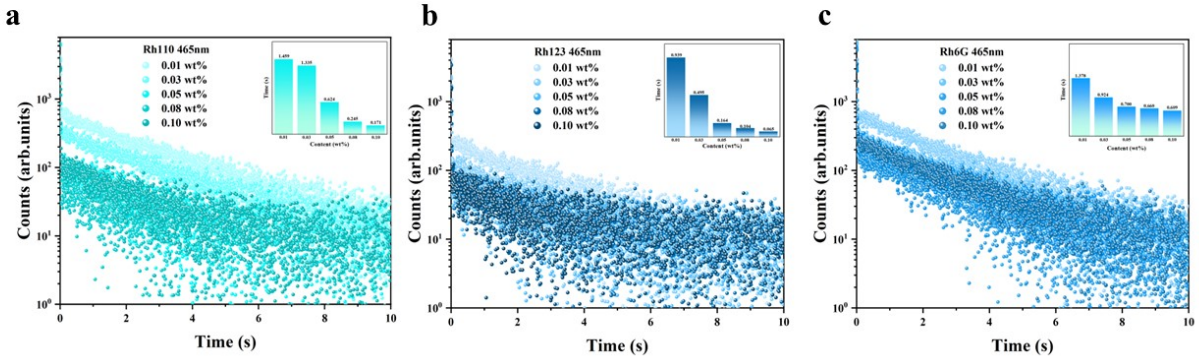

Figure S26. Lifetime decay profiles at 465 nm of afterglow films: (a) Rh110/1,4-BDBA @HPD/PMMA, (b) Rh123/1,4-BDBA @HPD/PMMA, and (c) Rh6G/1,4-BDBA @HPD/PMMA under 275 nm excitation.

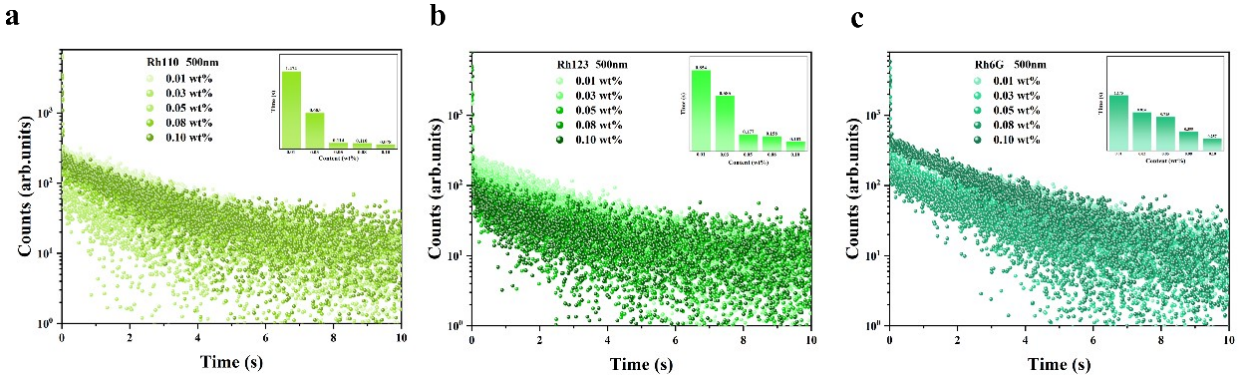

Figure S27. Lifetime decay profiles at 500 nm of afterglow films: (a) Rh110/1,4-BDBA @HPD/PMMA, (b) Rh123/1,4-BDBA @HPD/PMMA, and (c) Rh6G/1,4-BDBA @HPD/PMMA under 275 nm excitation.

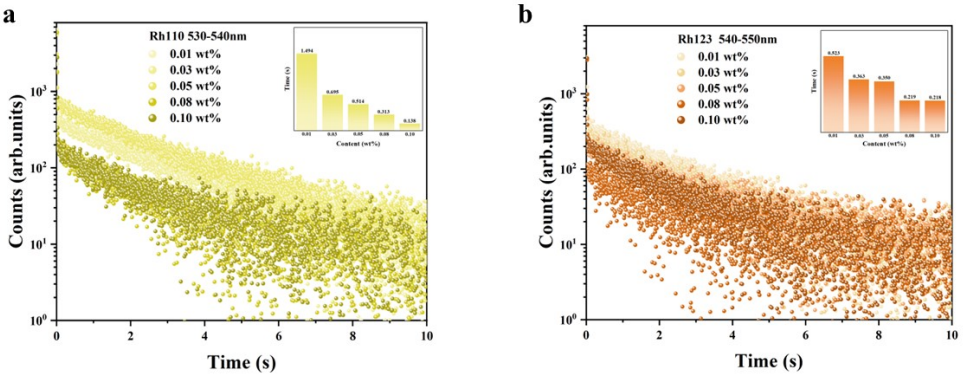

Figure S28. Lifetime decay profiles in wavelength ranges of (a) 530–540 nm and (b) 550–560 nm for afterglow films: (a) Rh110/1,4-BDBA @HPD/PMMA and (b) Rh123/1,4-BDBA @HPD/PMMA under 275 nm excitation.

Table S1. Summary of photophysical properties of 1,4-BDBA@HPD at room temperature.

Sample	λ_{em} (nm)	τ_p (s)	Φ_f (%)	Φ_p (%)	Φ_{isc} (%)	k_p (s^{-1})	$k_{p,nr}$ (s^{-1})
1,4-BDBA @HPD (1:2)	330	-					
	465	1.514	16.98	0.67	83.02	0.0053	0.66
	500	1.577					
1,4-BDBA @HPD (1:3)	330	-					
	465	2.368	22.94	1.20	77.06	0.0066	0.42
	500	2.274					
1,4-BDBA @HPD (1:4)	330	-					
	465	1.833	22.58	1.07	77.42	0.0075	0.54
	500	1.153					
1,4-BDBA @HPD (1:5)	330	-					
	465	1.574	18.32	0.55	81.68	0.0043	0.63
	500	1.448					
1,4-BDBA @HPD (1:6)	330	-					
	465	1.558	17.41	0.62	82.59	0.0048	0.64
	500	1.995					

Here, the $\Delta E_{S1-S0} = 1240/\lambda = 1240/450 = 2.76$ eV, the k_{ic} is approximately negligible.[2]

$$\Phi_{isc} = 1 - \Phi_f - \Phi_{f,nr} \approx 1 - \Phi_f$$

$$k_p = \Phi_p / (\Phi_{isc} \times \tau_p)$$

$$k_{p,nr} = \frac{1}{\tau_p} - k_p$$

Where λ_{em} refer to emission wavelength; τ_p refer to the lifetime of phosphorescence; Φ_f, Φ_p and Φ_{isc} refer to the quantum yield of fluorescence, phosphorescence and intersystem crossing; k_p refer to radiative decay rate of phosphorescence; $k_{p,\,nr}$ refer to nonradiative decay rate of phosphorescence.

Table S2. Energy transfer parameters between 1,4-BDBA@HPD (donor) and Rh110, Rh123 and Rh6G (acceptor).

Sample	wt. of dyes (%)	λ_{em} (nm)	$\tau_{p/f}$ (s)	$\Phi_{p/f}$ (%)	E_1 (%)	E_2 (%)	k_{FRET} (s^{-1})
1,4-BDBA @HPD/PMMA	-	465 500	1.517 1.778	5.96	-	-	-
Rh110/1,4-BDBA@HPD/PMMA	0.01	465 500 531	1.459 1.474 1.494	3.23	0.038	0.171	0.116
	0.03	465 500 536	1.335 0.683 0.695	6.96	0.120	0.616	0.902
	0.05	465 500 536	0.624 0.114 0.514	6.20	0.589	0.936	8.210
	0.08	465 500 540	0.245 0.110 0.313	5.30	0.838	0.938	8.528
	0.10	465 500 540	0.171 0.078 0.138	3.68	0.887	0.956	12.258
	0.01	465 500 540	0.939 0.854 0.523	6.73	0.381	0.520	0.609
	0.03	465 500 546	0.495 0.585 0.363	10.74	0.674	0.671	1.147

		465	0.164				
	0.05	500	0.177	11.70	0.892	0.900	5.087
		546	0.350				
		465	0.104				
	0.08	500	0.158	11.86	0.931	0.911	5.767
		548	0.219				
		465	0.065				
	0.10	500	0.102	8.37	0.957	0.943	9.241
		550	0.218				
		465	1.378				
	0.01	500	1.175	5.88	0.092	0.339	0.289
		560	0.657				
		465	0.924				
	0.03	500	0.814	11.41	0.391	0.542	0.666
		565	0.559				
Rh6G/1,4-		465	0.700				
BDBA@HPD/P	0.05	500	0.715	10.11	0.539	0.598	0.836
MMA		570	0.405				
		465	0.660				
	0.08	500	0.399	6.37	0.565	0.776	1.944
		571	0.195				
		465	0.609				
	0.10	500	0.257	14.68	0.599	0.855	3.329
		573	0.124				

$E = 1 - \tau_{D,A}/\tau_D$[3]

$$k_{FRET} = \frac{\left(\frac{R_0}{R}\right)^6}{\tau_D} = \frac{E}{\tau_D(1-E)}$$

$E = R_0^6/(R_0^6 + R^6)$

Where $\tau_{D,A}$ is the lifetime of donor in presence of acceptor; τ_D is the lifetime of donor without any acceptor; E is the energy transfer efficiency between the energy donor and acceptor (E_1:465 nm E_2: 500 nm); k_{FRET} is the rate of FRET from donor (500 nm) to acceptor (530-570 nm); R_0 and R refer to Förster critical transfer distance and Förster distance. The Förster radius (R_0) corresponds to the distance at which the FRET efficiency reaches 50%.

Table S3. Energy transfer radius between the donor (1,4-BDBA@HPD) and

acceptors (Rh110, Rh123 and Rh6G).

Samples	$J(\lambda)$(S-S) ($nm^4\ M^{-1}\ cm^{-1}$)	$J(\lambda)$(T-S) ($nm^4\ M^{-1}\ cm^{-1}$)	R(S-S) (Å)	R(T-S) (Å)
Rh110/1,4-BDBA@HPD/PMMA	3.597×10^{14}	1.359×10^{15}	23.81	29.71
Rh123/1,4-BDBA @HPD/PMMA	1.096×10^{14}	1.904×10^{15}	19.53	34.43
Rh6G/1,4-BDBA @HPD/PMMA	1.329×10^{14}	2.349×10^{15}	20.17	32.55

Sample	wt. of dyes (%)	CIE coordinates
1,4-BDBA@HPD-293K	-	(0.18, 0.36)
1,4-BDBA @HPD-77k		(0.15, 0.12)
Rh110/1,4-BDBA @HPD/PMMA	0.01	(0.20, 0.40)
	0.03	(0.24, 0.45)
	0.05	(0.23, 0.45)

$$R^6 = 8.8 \times 10^{-5}\left[\kappa^2 n^{-4} \Phi_D J(\lambda)\right]$$ [3]

where κ represents the orientation factor of a molecular dipole, n is the refractive index of the polymer host (PMMA), Φ_D is the quantum efficiency of the donor, J(λ) is the overlap integral between donor emission and acceptor absorption, which can be calculated from the normalized emission spectrum of the donor with absorption spectra in molar absorptivity of the acceptors on a|e 1.2 FluorTools software.[4]

In this work, $\kappa^2 = 0.476$ as we assume the luminophores to be well-separated and randomly oriented during excitation, n = 1.49 and Φ_D (Phosphorescence) =5.96%. The calculated distances are well satisfied with the basic requirement of the FRET process with the energy transfer distance between 5 and 100 Å to maintain effective FRET from the phosphorescent donor to fluorescent acceptor.[5]

Rh123/1,4-BDBA @HPD/PMMA	0.08	(0.30, 0.49)
	0.10	(0.30,0.48)
	0.01	(0.27, 0.49)
	0.03	(0.33, 0.50)
	0.05	(0.33, 0.54)
	0.08	(0.33, 0.52)
	0.10	(0.37, 0.54)
Rh6G/1,4-BDBA @HPD/PMMA	0.01	(0.26,0.38)
	0.03	(0.31, 0.40)
	0.05	(0.35, 0.40)
	0.08	(0.37, 0.41)
	0.10	(0.40, 0.42)

Table S4. 1931 CIE coordinates of delayed photoluminescence spectra of different samples.

References

[1] Gaussian 09, Revision A.02, M. J. Frisch, G. W. Trucks, H. B. Schlegel, G. E. Scuseria, M. A. Robb, J. R. Cheeseman, G. Scalmani, V. Barone, G. A. Petersson, H. Nakatsuji, X. Li, M. Caricato, A. Marenich, J. Bloino, B. G. Janesko, R. Gomperts, B. Mennucci, H. P. Hratchian, J. V. Ortiz, A. F. Izmaylov, J. L. Sonnenberg, D. Williams-Young, F. Ding, F. Lipparini, F. Egidi, J. Goings, B. Peng, A. Petrone, T. Henderson, D. Ranasinghe, V. G. Zakrzewski, J. Gao, N. Rega, G. Zheng, W. Liang, M. Hada, M. Ehara, K. Toyota, R. Fukuda, J. Hasegawa, M. Ishida, T. Nakajima, Y. Honda, O. Kitao, H. Nakai, T. Vreven, K. Throssell, J. A. Montgomery, Jr., J. E. Peralta, F. Ogliaro, M. Bearpark, J. J. Heyd, E. Brothers, K. N. Kudin, V. N. Staroverov, T. Keith, R. Kobayashi, J. Normand, K. Raghavachari, A. Rendell, J. C. Burant, S. S. Iyengar, J. Tomasi, M. Cossi, J. M. Millam, M. Klene, C. Adamo, R. Cammi, J. W. Ochterski, R. L. Martin, K. Morokuma, O. Farkas, J. B. Foresman, and D. J. Fox, Gaussian, Inc., Wallingford CT, 2016.

[2] Hirata, S. Roles of Localized Electronic Structures Caused by π Degeneracy Due to Highly Symmetric Heavy Atom-Free Conjugated Molecular Crystals Leading to Efficient Persistent Room-Temperature Phosphorescence. Advanced Science 6 (2019). https://doi.org:10.1002/advs.201900410

[3] Gong, Y. et al. Achieving Persistent Room Temperature Phosphorescence and Remarkable Mechanochromism from Pure Organic Luminogens. Advanced Materials 27, 6195-6201 (2015). https://doi.org:10.1002/adma.201502442
[4] a|e - UV-Vis-IR Spectral Software 1.2, FluorTools, http://www.fluortools.com.
[5] Zou, X. et al. Narrowband Organic Afterglow via Phosphorescence Förster Resonance Energy Transfer for Multifunctional Applications. Advanced Materials 35 (2023). https://doi.org:10.1002/adma.202210489